ELKHORN SLOUGH
TECHNICAL REPORT SERIES 2020: 1

Sponsored by the Elkhorn Slough National Estuarine Research Reserve and the Elkhorn Slough Foundation

Hester Marsh Salinity Report

Johannes Krause

May 2020

HOW TO CITE THIS DOCUMENT

The appropriate citation for this document is:

Krause, J. R. 2020. Hester Marsh Salinity Report. Elkhorn Slough Technical Report Series 2020:1. Available at http://www.elkhornslough.org/research-program/technical-report-series/

AUTHOR AFFLIATION

Johannes Krause conducted this research while a student supervised by Dr. Elizabeth Watson at Drexel University. The work was partially funded by the Elkhorn Slough National Estuarine Research Reserve.

DISCLAIMER

ABOUT THE ELKHORN SLOUGH TECHNICAL REPORT SERIES

The mission of the Elkhorn Slough Foundation and the Elkhorn Slough National Estuarine Research Reserve is conservation of estuarine ecosystems and watersheds, with particular emphasis on Elkhorn Slough, a small estuary in central California. Both organizations practice science-based management, and strongly support applied conservation research as a tool for improving coastal decision-making and management. The Elkhorn Slough Technical Report Series is a means for archiving and disseminating data sets, curricula, research findings or other information that would be useful to coastal managers, educators, and researchers, yet are unlikely to be published in the primary literature.

Abstract

The magnitude and spatial distribution of soil salinity was predicted at the Hester marsh restoration site (Elkhorn Slough, CA), where sediment was recently added to raise the elevation of the marsh plain. Field measurements of apparent bulk conductivity using a portable conductivity meter (EM38 MK2) were related to soil salinity by generating calibration curves, for two sampling campaigns at the start and end of the summer dry season. To aid spatial modelling of soil salinity, a UAV survey was conducted, and the resulting multispectral imagery was used to derive elevation, vegetation, and soil moisture information. Additional spatial data relating to elevation change and distance to tidal channels were included in a partial least squares regression model ($R^2 = 0.86$, RMSE = 5 ppt). Model predictions of salinity increase with proximity to tidal channels and at low elevations, while lower predicted salinity corresponds to previously high elevation sites where sediment was removed for restoration. For a given elevation, soil salinity was lower at the start of the dry season (April) compared to the end of the dry season (September). The methodology presented herein is suitable for regular monitoring of marsh soil salinity, as field work can be minimized using the portable EM38 MK2 and UAV. The resulting data can inform investigations into the recolonization of coastal wetland vegetation in restoration projects, as well as coastal wetland health and plant distribution patterns more generally.

Introduction

Tidal salt marshes are valuable habitats that provide ecosystem services, such as flood protection, nutrient removal, food and nursery habitat for numerous species, as well as carbon sequestration (Costanza *et al.*, 1997; Kennish, 2001). However, salt marshes are disappearing globally, due to various stressors, including human development, nutrient over-enrichment, loss of sediment supply, and sea level rise (Craft *et al.*, 2009). The latter two stressors directly affect the elevation of a marsh relative to sea level, which is of importance, because the area inhabited by emergent salt marsh vegetation is typically limited by hydroperiod and inundation time. Different salt marsh plant species show varying degrees of tolerance for flooding, which governs

root-zone aeration and soil sulfide levels, as well as soil salinity (Bertness, 1991). The latter can be an important factor influencing salt marsh plant health, by causing physiological stress, through its influence on nitrogen availability, or by reducing the competitiveness relative to organisms adapted to a different soil salinity regime.

The salinity of marsh soils can be determined by soil and porewater sampling followed by laboratory analysis. To measure salinities over a large area, this approach is impractical. An alternative approach is to measure the conductivity of marsh soil and ascertain the relationship of conductivity to soil salinity. Portable electromagnetic induction instruments are a common tool in agricultural studies and have the advantage of delivering instantaneous, continuous measurements of a metric closely related to salinity, apparent conductivity. A conductivity meter consists of at least two coils positioned a fixed distance apart, which can produce a magnetic field when energized with an alternating current. When positioned close to the earth, the magnetic field produced by the transmitter coil induces small electrical currents in the soil. These in turn generate a secondary magnetic field, which can be sensed by the receiver coil. The secondary magnetic field is a function of the distance between coils, the operating frequency of the instrument, and the ground conductivity (McNeill, 1980). The latter is mainly influenced by soil water content, soil composition and density, and salinity (Corwin and Lesch, 2005). For salt marshes with homogenous mineralogy and hydrodynamics, apparent conductivity should be a strong predictor for salinity.

This project aims to measure apparent conductivity of a tidal salt marsh, create calibration curves to derive soil salinity, and predict soil salinity over the spatial extent of the marsh.

Methods

Study Site

The present study was carried out at the Hester Marsh restoration site in Elkhorn Slough, Monterey Bay, CA. This tidal salt marsh was constructed to rebuild an area of coastal marsh that was degraded by levee construction. Between 1931 and 1949, the area was diked and impounded. Once the area was re-exposed to tidal exchange in the 1980s, the ground had subsided due to dewatering and consolidation, and the area was too low in elevation and flooded too frequently to support healthy marsh plants. Rather, mudflats characterized by blooms of opportunistic macroalgae and low invertebrate diversity were established. A significant portion of Elkhorn Slough marshes have drowned over the past decades (Van Dyke and Wasson, 2005), even those that were not previously diked. Low water column suspended sediment concentrations prevent high rates of vertical marsh accretion through sediment trapping, so managers chose to focus on rebuilding a high elevation marsh. The goal of this project was to construct a marsh that would persist under predicted rates of sea level rise over coming decades and also include a regrading component to insure that the marsh would be able to migrate into adjacent grasslands even if it was not able to persist in its current footprint. To inform studies of wetland plant recolonization, spatial patterns in soil salinity were investigated.

Field sampling procedure

Field sampling of apparent conductivity took place in April and September 2019, at the beginning and end of the dry season, respectively. Apparent conductivity was measured using a Geonics Model EM38 MK2 Conductivity Meter (Geonics Ltd, Mississauga, Ontario, Canada) and recorded on a handheld GPS unit (Garmin GPSMAP 64ST, Garmin Ltd, Olathe, Kansas, USA). In April and September, 10 pre-established monitoring transects (length 60 – 200 m) were surveyed at equal intervals of approximately 5 m. In September, additional sampling included six

30 m by 35 m plots where different native marsh plant species where planted along an elevation gradient, as well as 30 sites destined for soil analysis (Fig. 1).

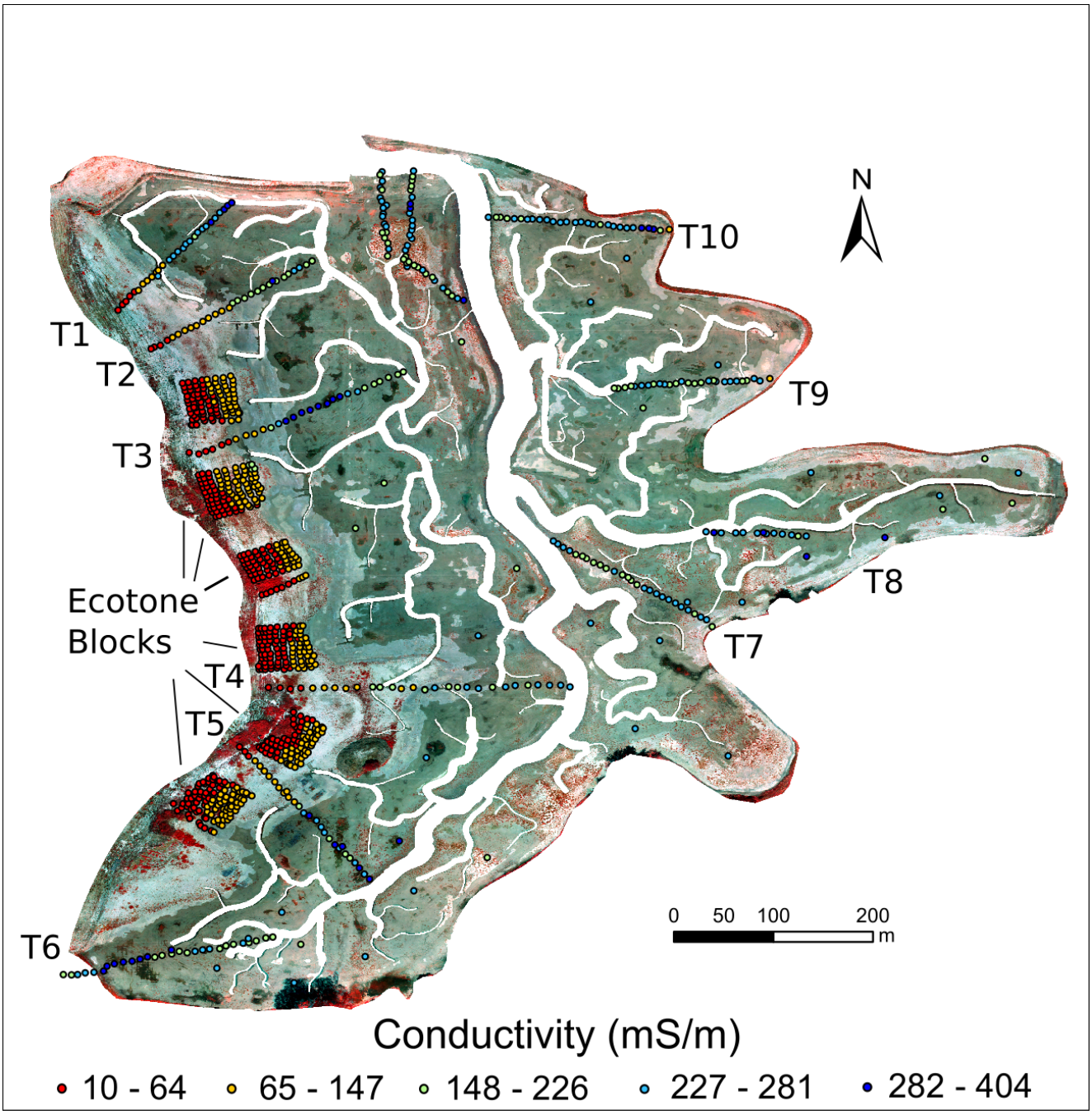

Figure 1: Field sampling locations for apparent conductivity in September 2019 over a false-color representation of the UAV-derived multispectral orthomosaic of Hester Marsh.

The conductivity meter was operated in vertical mode, with a coil spacing of 0.5 m, to measure apparent conductivity to a depth of 0.75 m from coil. Held 60 cm above the ground, the resulting EC_a reading represents the top 15 cm of marsh soil. Additionally, horizontal readings with 0.5 m inter-coil distance were taken at regular intervals, with the instrument positioned directly on the ground, measuring the top 0.38 cm of soil. Before each survey, the operator removed all metal objects to avoid interference. The instrument was zeroed at the beginning of each day and every 4 hours on site, following the manufacturer's instructions.

Marsh surface soil samples were collected in April (n = 8) and September (n = 22) for salinity determination using a push corer. Samples were stored frozen and shipped to the Academy of Natural Sciences of Drexel University for laboratory analysis.

Drone flights

In September 2019, a UAV equipped with RGB camera (DJI Phantom 4 Pro; SZ DJI Technology Co., Shenzhen, China) and near-infrared (NIR) sensor (Sentera Inc, Minneapolis, USA) was used to gather imagery of the marsh surface. Flying at an altitude of 61 m, the ground resolution of each image was 5.6 cm per pixel. Additionally, two regions of interest were surveyed at 30 m altitude, resulting in an image resolution of 2.8 cm per pixel. All surveys were performed in low-wind conditions between 10 am and 4 pm, with a minimum overlap between images of 70 % and at speeds less than 16 km/h.

Laboratory analysis

To determine the water content of each soil sample, a volume of 2.5 cc was weighed wet and dry after overnight drying in an oven heated to 105°C. Additional RO-water was added, so that each sample reached a water to soil ratio of 5:1 by mass. Samples were subsequently shaken for one minute, centrifuged at 2000 rpm for 5 minutes, and the salinity was measured on the supernatant using a YSI Pro 2030 with conductivity probe (YSI Inc, Yellow Springs, Ohio, USA). One third of samples were run in duplicate to estimate repeatability. For final salinity

values, the amount of water added to each sample was corrected for, so that salinity reported here corresponds to the original moisture content.

An additional 30 soil samples were obtained on October 2nd 2019 and analyzed for a range of soil chemistry parameters as well as granulometry by a third party laboratory. These independently analyzed samples were tested for possible correlations of soil characteristics and field measurements of apparent conductivity.

Drone imagery processing

UAV images were processed in Agisoft Metashape v1.5 (Agisoft LLC, St. Petersburg, Russia), following a workflow of image quality control, image alignment, removal of points with poor accuracy, dense point cloud generation, mesh generation, texture mapping, digital elevation model (DEM) generation (Fig. 2 b), and orthomosaic generation. High-accuracy ground control points were previously established at the study site using a laser level. These were utilized for DEM creation and georeferencing in this study.

Furthermore, dense point clouds of the two areas of interest were classified in ground points and other points using Metashape built-in classification tools, to create DEMs from ground points only, to test the removal of elevation bias caused by vegetation. The 'classify ground points' tool splits the point cloud into quadratic subsets, for which a plane representing the ground is identified. Points close to that plane are classified as ground points, with a set of tunable parameters defining the thresholds for what constitutes a ground point. The tunable parameters for ground point classification are 'max angle', which defines the maximum slope of the ground, 'max distance', which determines the maximum variation in ground elevation, and 'cell size', which determines the size of quadratic subsets of the point cloud. DEMs based on ground points only were compared to those including vegetation points by subtracting one raster from another, effectively calculating vegetation heights.

UAV-derived imagery was further processed to create a multispectral orthomosaic (Fig. 1), as well as spectral indices. The NIR reflectance was extracted from the NIR orthomosaic following the sensor manual, co-registered with the RGB orthomosaic, and added to the RGB bands to create a composite multispectral raster file in ENVI 5.4 (L3Harris Geospatial, Boulder,

CO). The soil moisture index (SMI, Fig. 2 c) and normalized difference vegetation index (NDVI, not shown) were calculated using the following equations:

$$(1)\ SMI = \frac{NIR}{Blue}$$

$$(2)\ NDVI = \frac{NIR-Red}{Nir+Red}$$

In ArcMap 10.6 (ESRI, Redlands, CA), a raster file with pixel values for the distance to the nearest channel was created using the Euclidian Distance tool and an input shapefile of current channel positions (Fig. 2 a). Additionally, a raster file indicating the elevation change resulting from sediment addition and removal associated with construction of the new marsh platform was made available by ESNERR and was incorporated in subsequent analyses (Fig. 2 d). Spatially referenced apparent conductivity readings and modelled salinity values, as well as the spatial data layers (Fig. 2) were imported to R Studio (v. 1.2.5033) for data analysis.

Data Analysis

All data analyses were performed in R version 3.3.2 (R core team 2016). To estimate soil salinity (ppt) from apparent conductivity (mS/m), three calibration functions were fit for laboratory-derived soil salinity values and conductivity field measurements from April and September in horizontal and vertical instrument mode, respectively. Visual evaluation of scatterplots led to testing of several candidate functions, of which the one with highest coefficient of determination was selected and used to model salinity (ppt) data for every apparent conductivity reading.

To predict soil apparent conductivity across the entire spatial extent of Hester marsh, multiple predictive models were tested. First, linear models were implemented using the independent variables elevation (UAV-derived DEM), distance from channel, and SMI to predict conductivity, utilizing the *caret* package version 6.0-86 (Kuhn, 2008). Second, a partial least squares regression (PLSR) model was tested, utilizing the package *pls* 2.7-2 (Wehrens and Mevik, 2007). This method derives latent variables (components), each describing as much covariance between the predictors and observations as possible.

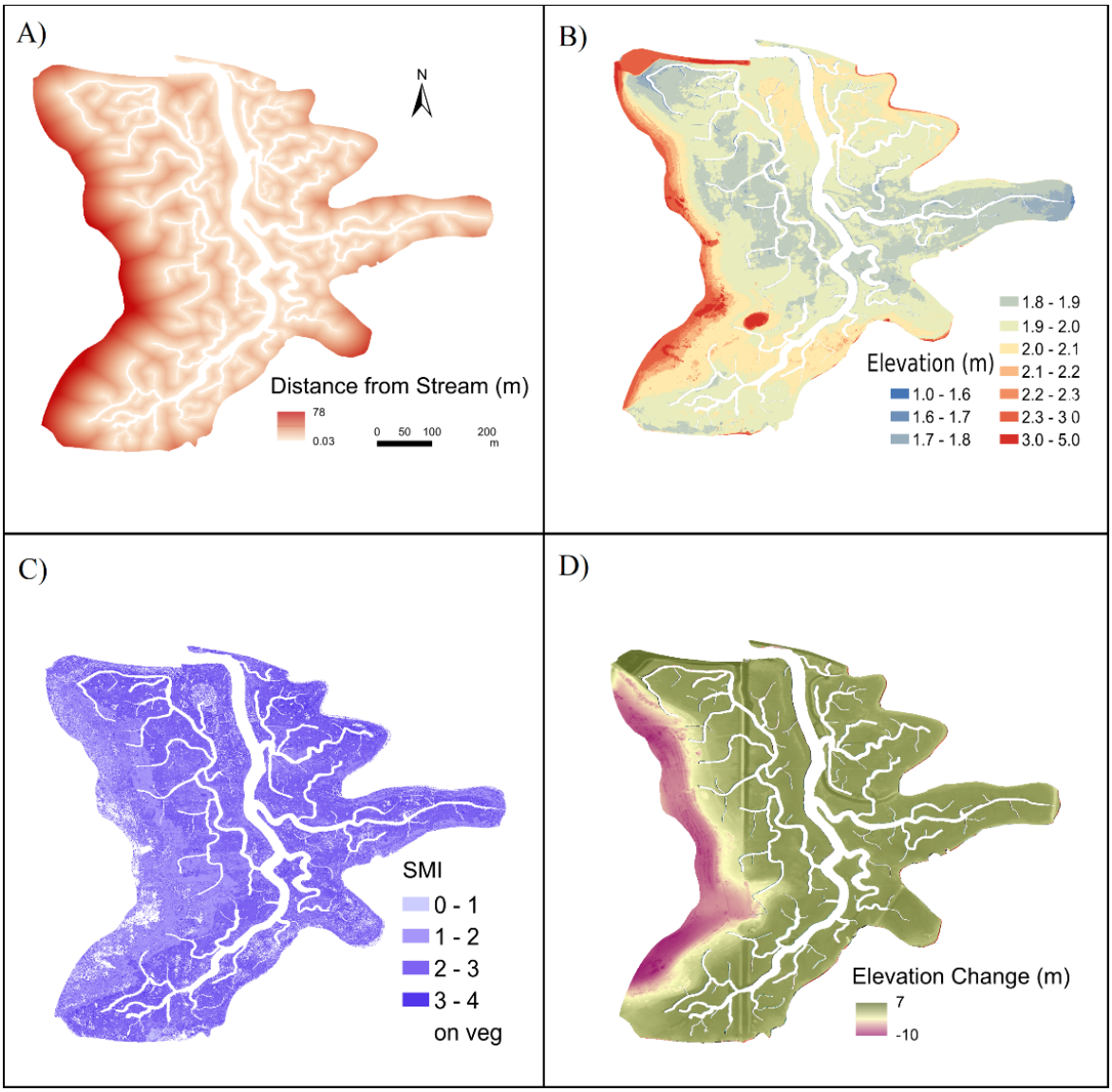

Figure 2: GIS layers used for predicting conductivity; A) Distance from stream (m), B) UAV-derived elevation (m), C) Soil Moisture Index, and D) Elevation change (m).

The number of components to include in the model is selected to minimize the root mean square error of prediction (RMSEP) after cross-validation and to maximize how much of the variance of the response variable is explained. In order to aid variable selection for PLSR, the relative importance of each variable is assessed by calculating variable importance in the projection (VIP) metrics. The VIP score indicates what fraction of the variance captured by latent variables is explained by each predictor variable, with VIP > 1 signaling high importance.

Spatial data handling and writing of prediction raster were performed using *sp* 1.4-1 (Pebesma and Bivand, 2005) and *raster* 3.0-12 (Hijmans *et al.*, 2019).

Results

Apparent conductivity

In September 2019, apparent conductivity readings obtained with the EM38 MK2 ranged from 10 mS/m to 404 mS/m, with lowest conductivities located on the westernmost quadrats on transects 1 to 5 (T1 – T5, Fig. 1) and at the higher elevation ecotone plots. Conductivity gradients were observed to correspond with elevation on the ecotone plots, so that higher elevation samples generally have a lower conductivity (Fig. 1). Additionally, conductivity gradients are present on the sampled transects, with transects 1 – 5 generally showing an increase in conductivity from west to east and in proximity to tidal channels. There was no clear gradient on transects 6 – 10, where variation in apparent conductivity does not follow a clear spatial pattern. Across the marsh, those sites where sediment was removed show lower conductivity than sites where sediment was added.

April conductivity measurements only took place at the transects and not at the ecotone planting blocks. Generally, apparent conductivity was lower in April (-27 – 377 mS/m), but spatial patterns of variability mirror those reported for September, with a gradual increase of conductivity from west to east in transects 1 – 5 and more homogenous measurements along transects 6 – 10. For a given elevation, apparent conductivity (and by extension salinity) was lower in April than in September (Fig. 3). September salinities were highest in those samples that had the lowest elevation, which correspond to sites with positive elevation change, where the restoration activities included sediment deposition onto the marsh. For a given elevation, September salinities were higher in samples from these sites compared to sites where sediment was removed (negative elevation change).

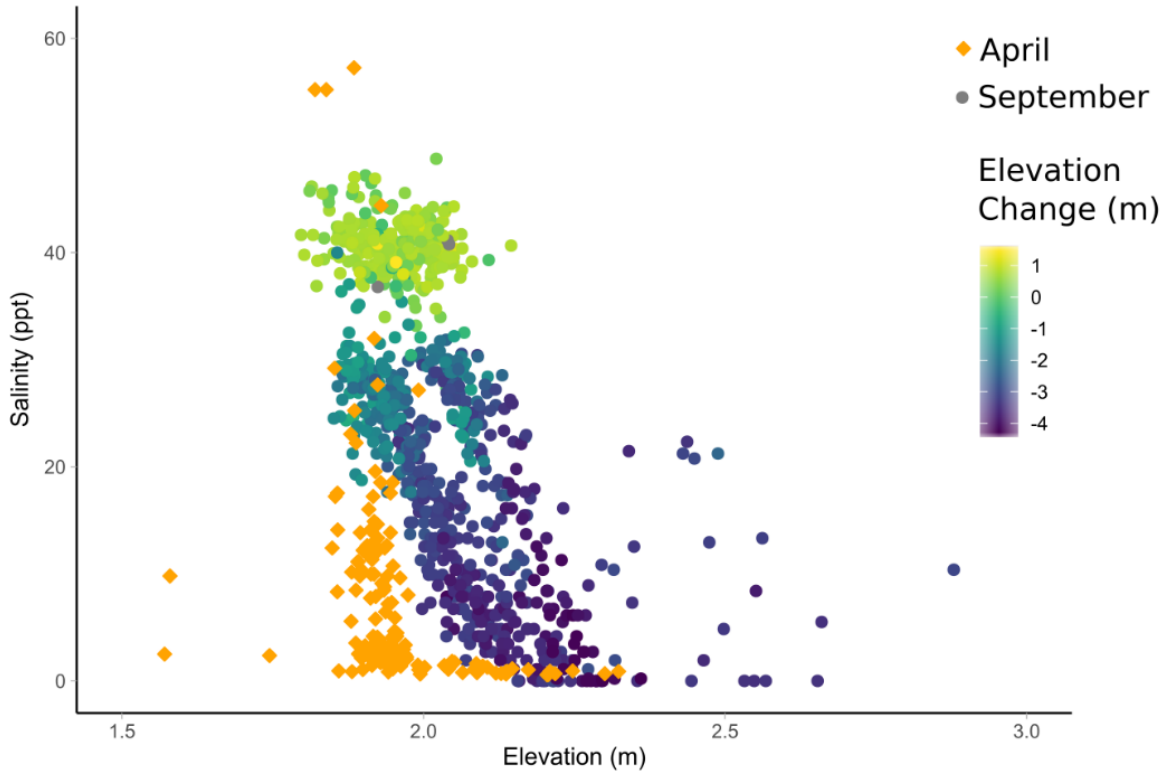

Figure 3: Modelled salinity for a given elevation in April (orange diamonds) and September (circles with color gradient indicating elevation change (m)).

Independently analyzed soil geochemical characteristics of 30 samples were tested for correlations with field measurements of apparent conductivity (Fig. 4). Field conductivity measurements show a positive correlation with soil moisture content and saturation (%). A positive correlation with mean grain size (φ) suggests higher apparent conductivity in the presence of finer sediments, which range from a bulk mean grain size of fine sand (φ = 2) to silt (φ = 5). There was no correlation between apparent conductivity field measurements and independent laboratory measurements of electrical conductivity (Fig. 4).

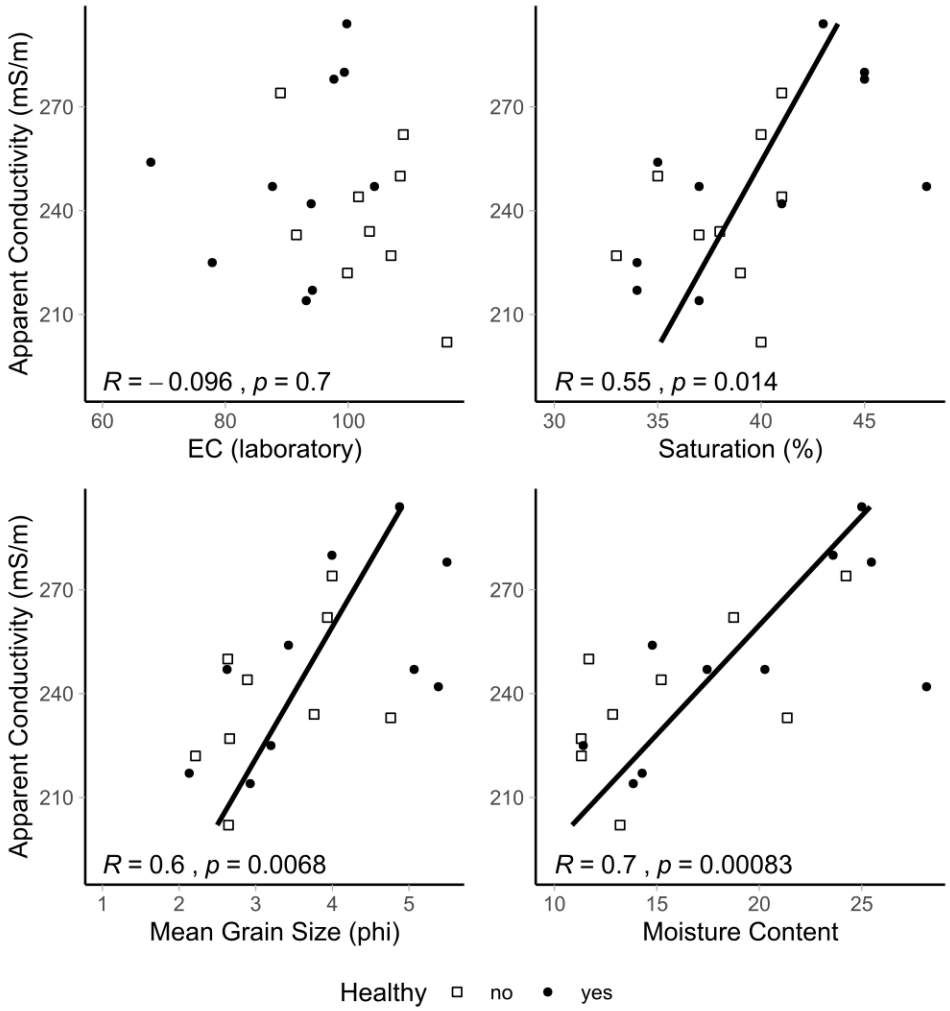

Figure 4: Apparent conductivity measurements from September 2019 and selected soil geochemical characteristics EC (top left), saturation (top right), mean grain size of bulk sediments (bottom left), and moisture content (bottom right). Point shapes indicate whether vegetation at the soil sampling sites was categorized as healthy (•) or not healthy (□). Linear regression lines drawn for significant correlations only.

Salinity at Hester Marsh

Hester marsh surface sediments collected in September 2019 were analyzed for salinity, which ranged from 0.2 to 71.2 ppt, with an average measurement error on duplicate samples of 0.5 ppt. The relationship of salinity to apparent conductivity was best described by an exponential function for data collected in April (Fig. 5 c, $R^2 = 0.80$) and September and for horizontal (Fig. 5 b, $R^2 = 0.85$) as well as vertical (Fig. 5 a, $R^2 = 0.80$) instrument modes. September apparent conductivity measurements in horizontal and vertical mode showed a high correlation (Fig. 5 d, $R^2 = 0.86$), indicating that conductivity patterns prevail when measurements

integrate a larger volume of soil. The calibration curves resulting from these empirical relationships of conductivity and soil salinity were used to model soil salinity for all conductivity sampling locations. While the soil samples used to derive calibration curves were relatively evenly distributed across the range of salinity values in September, the April samples mostly represented soil salinities of 10 ppt or less (Fig. 5 c). Therefore, the calibration of higher apparent conductivity readings for April is less constrained (as indicated by a larger confidence interval around the calibration curve) and high salinity estimates for this month should be treated with caution.

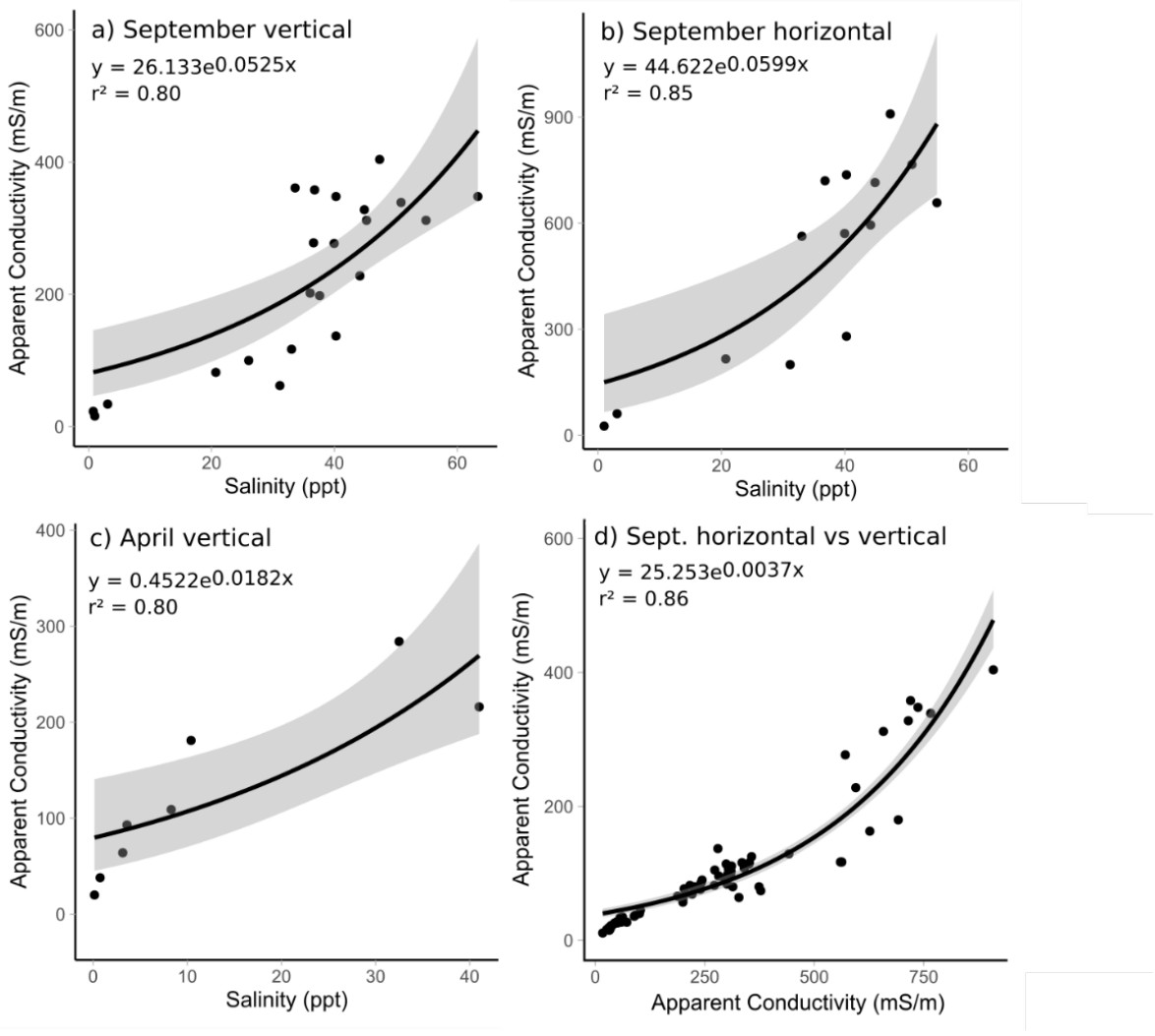

Figure 5: Calibration curves for salinity and apparent conductivity readings from (a) September, in vertical mode; (b) September, in horizontal mode; (c) April, in vertical mode; d) shows the relationship of Septermber vertical readings (y-axis) to horizontal readings (x-axis).

Predicting soil salinity

Linear regression models revealed a positive relationship of soil salinity to elevation change ($R^2 = 0.82$, $p < 0.0001$), with higher salinity at sites where sediment was added and lower salinity where sediment was removed by scraping the marsh-adjacent hillside. Furthermore, a negative linear relationship of soil salinity with distance from channel ($R^2 = 0.79$, $p < 0.0001$) was found, as well as a negative correlation with weaker explanatory power for salinity and elevation ($R^2 = 0.45$, $p < 0.0001$). Interactions were found for the variables elevation, distance from channel, and elevation change, suggesting their autocorrelation. A linear model predicting salinity with distance from channel and interaction terms of distance from channel, elevation, and elevation change had the highest explanatory power of the models tested ($R^2 = 0.88$, $p < 0.0001$):

$$Salinity = 23.1 \pm 10.4 + 2.1 \pm 0.6 \times Dist + 0.4 \pm 0.2 \times Dist * Change - 1.1 \pm 0.3\, Dist * Change * DEM$$

where *Dist* is distance from channel (m), *Change* is elevation change (m), and *DEM* is elevation (m).

The predictor variables described above show some degree of collinearity, especially elevation, distance from channel, and elevation change (Fig. 6 a). To circumvent the problem of collinearity of predictor variables when modeling conductivity, a partial least squares regression approach was implemented. A two-component model (R^2=0.86, RMSE: 5, diagnostic plots in Fig. 6 b and c) was selected to compute a raster file of predicted soil salinity (Fig. 7). The VIP metric identified the most important variables as distance from stream (VIP = 1.88) and elevation change (VIP = 0.68).

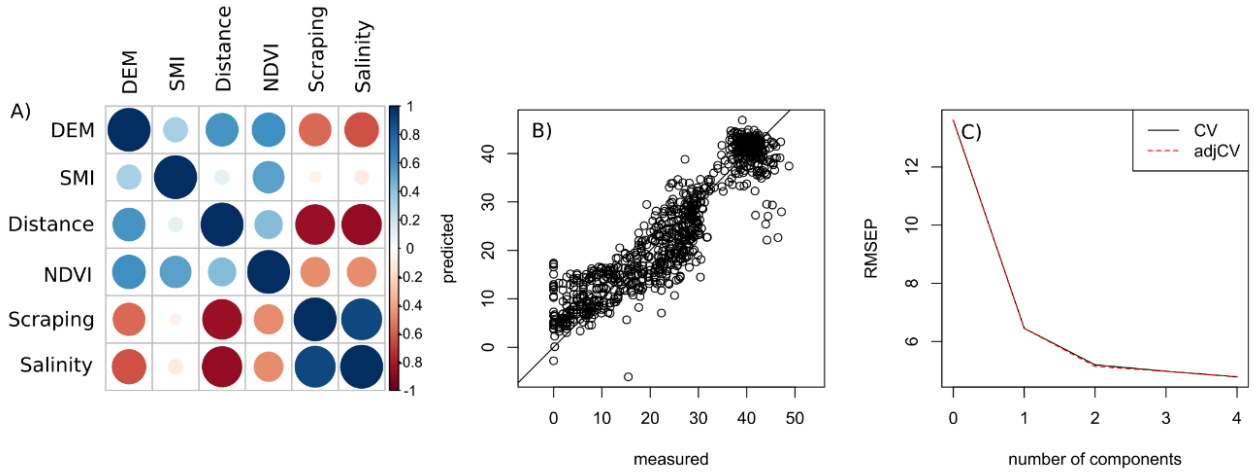

Figure 6: Salinity model evaluation plots: A) Correlation matrix of model parameters. Negative correlations are indicated by red circles, positive correlations are indicated by blue circles. Panel B) shows the September measured conductivity (expressed as salinity) values against the PLSR model prediction roughly falling on a 1:1 line. In C), the RMSE of PLSR prediction is shown for models with different numbers of latent variables (components). Including more than two components does not decrease RMSEP significantly.

Reducing vegetation bias in UAV-derived DEMs

The 'classify ground points' tool in Agisoft Metashape was tested with incrementally increasing threshold values for the parameters 'max distance', 'max angle', and 'cell size'. The ability of the algorithm to exclude vegetation increased with decreasing classification parameter 'cell size', with a 4 x 4 m cell omitting the most vegetation points. The parameter with most influence over point classification quality was 'max distance', with distance as little as 0.1 m classifying all vegetation as ground, while a distance of 0.05 m correctly omitted most vegetation points. It was not possible to generate a satisfactory point cloud classification for all of the marsh, but the resulting DEM bias decrease for a subset of the study site is shown (Fig. 8). It should be noted that the growth form and height of vegetation determines the success of this technique, with very small cell size and 'max distance' parameters leading to long processing times. With a more powerful processor, the approach presented here could be used to generate a digital terrain model, as well as to determine vegetation height. The latter is useful for monitoring recolonization of marsh plants and could be empirically related to other parameters, such as plant biomass or carbon burial.

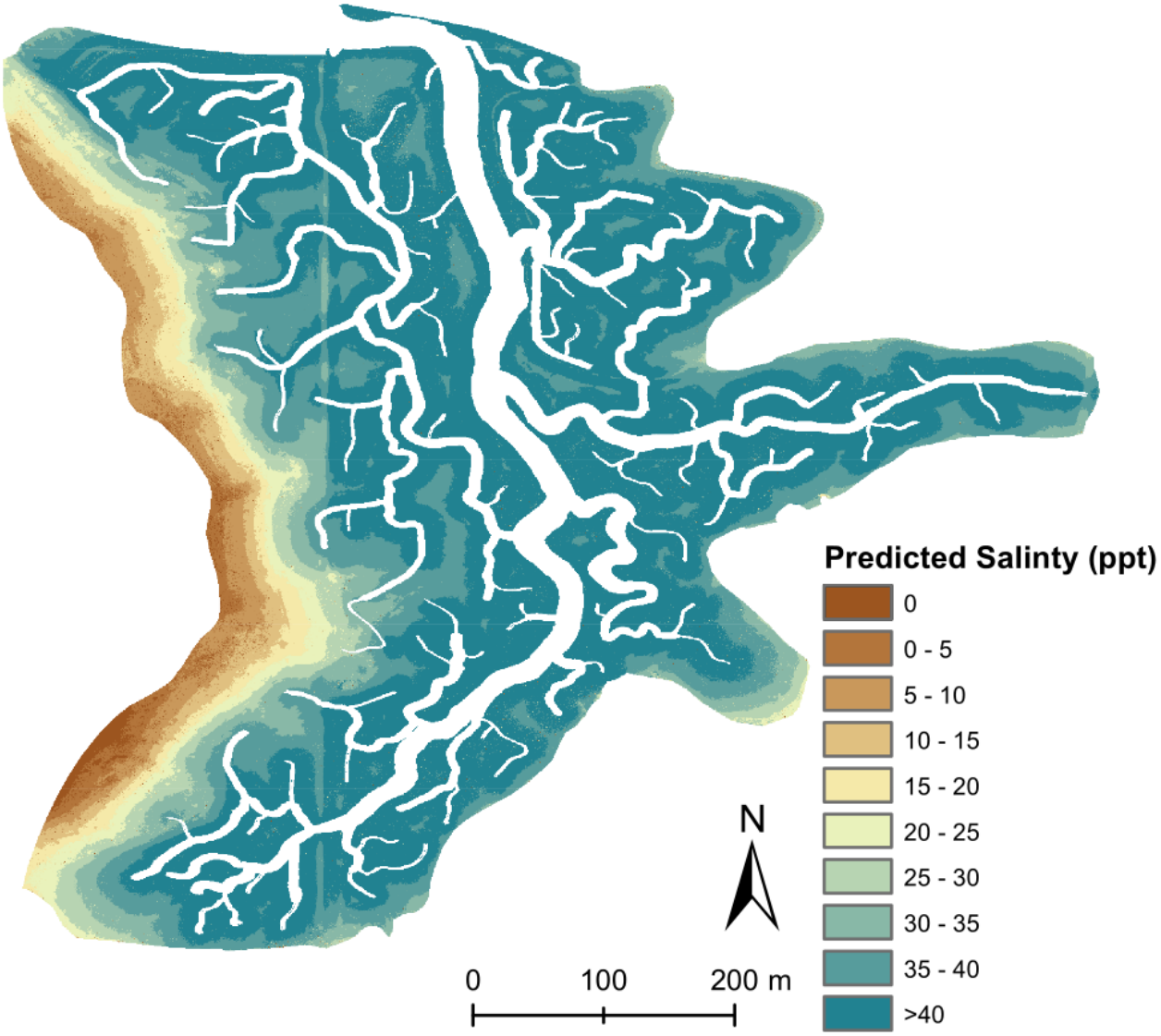

Figure 7: Soil salinity at Hester marsh in September 2019, as predicted by the PLSR model. Highest salinity values (> 40 ppt) are predicted near channels, with lowest salinities (0 – 10 ppt) at high elevation regions where sediment was removed for marsh restoration.

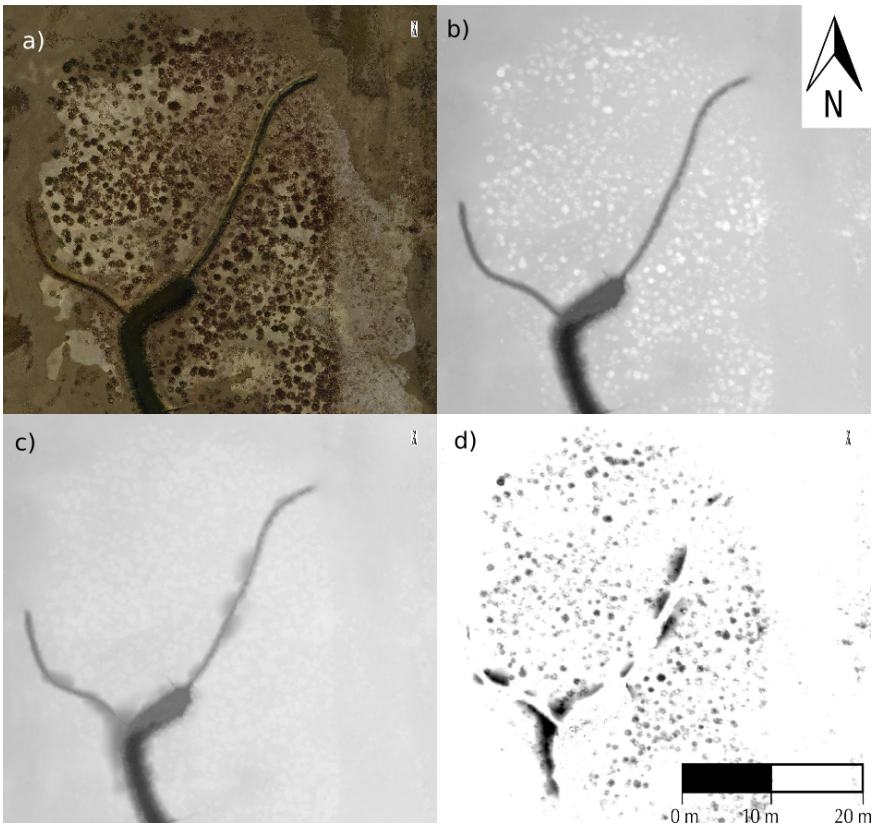

Figure 8: Plant elevation bias in DEM of densely vegetated region near the mouth of the main channel. AUV-derived orthomosaic (a) reveals vegetation presence. The corresponding DEM without point cloud classification (b) shows higher elevation where plants are present (white). A DEM post-point cloud classification (c) reveals a more homogenous elevation distribution. The difference in elevation of both DEMs is shown in (d), where darker colors indicate a larger difference in elevation, or plant height. The dark circular objects are areas in which vegetation leads to an overestimation of marsh elevation.

Discussion

Soil salinity

Lower conductivity measurements for a given elevation in April compared to September could be a result of reduced soil salinity due to rainfall. As April marks the end of the wet season in the study region, while the dry season ends in September, differences in soil salinity could be expected. The difference between months is especially apparent for samples with an elevation of > 2 m (Fig. 3). Marsh soil at lower elevations may be more regularly affected by tidal inundation, which increases cation concentrations in April as well as September, while the salinity of higher elevation soil could be more influenced by precipitation. A previous study in tidal wetland soils

found that 6-month cumulative rainfall can be an important predictor of soil electromagnetic conductivity (McKinney *et al.*, 2019)

Electromagnetic conductivity is also a function of soil type, in that mineral and clay content influence conductivity readings regardless of porewater salinity (Corwin and Lesch, 2005). If different soils were present at the surface of Hester marsh, this could have decreased the explanatory power of the calibration functions. Apparent conductivity readings were higher where mean grain size was small (see Fig. 4), indicating soil type had an effect on field measurements. There was no data available for the full spatial extent of the study site, so this factor did not form part of the salinity predictions presented herein. Future models could be improved by introducing information on the spatial distribution of soil characteristics, when such data are available.

UAV products

The methodology presented here makes use of a UAV with multispectral sensors to collect spatial information regarding vegetation location and density, soil moisture, and elevation. All independent variables used for modelling salinity in this study can be obtained simultaneously and almost at the same time as the soil samples and conductivity readings. This integrated workflow allows for a swift data acquisition that can be easily repeated several times per season and lends itself for a seasonal sampling.

Since soil moisture content is one of the factors governing soil conductivity, a soil moisture index was included in spatial modelling of conductivity. Utilizing an UAV fitted with an appropriate sensor, it is feasible to obtain soil moisture indices at the time of sampling conductivity and across the entire study area. The SMI layer calculated in this study displays higher values in locations that were recently inundated. However, SMI data had no significant correlation with conductivity and was not found to be an important variable for the PLSR model (VIP = 0.3). This apparent lack of predictive power could be attributed to a number of factors. Firstly, the SMI used here is based solely on the blue and NIR bands, with the latter being influenced by factors other than moisture, for example by the presence of chlorophyll. Second, soil moisture indices should only be calculated over bare ground, while there is some vegetation

cover in parts of the study site. To allow for the use of a soil moisture index for conductivity mapping, data processing should include masking of vegetation. Ideally, a sensor measuring short-wave infrared instead of near-infrared would allow for more refined soil moisture indices to be derived, such as NINSOL (Fabre, Briottet and Lesaignoux, 2015)

The DEM obtained from a structure-from-motion workflow using UAV images initially differed significantly from previously generated DEMs of the same site. Comparing elevations of ground control points with DEM values at the same locations revealed a doming effect of the DEM, resulting from poorly estimated lens distortion parameters. Alternative lens distortion parameters were derived using the doming analysis tool 1.0 (James and Robson, 2014) with ground control points that were not used in the initial DEM generation. After correcting for this effect, RMSE was 0.06 m, with the largest deviation of DEM value from laser-levelled control points of 0.13 m.

Predicted salinity

Even though individual spatial data products like DEM, NDVI, and SMI maps leave room for improvement, in combination with spatial informatin of elevation change and distance from channels, they allowed for predictive modelling of soil salinity at Hester marsh. Linear regression analysis revealed a negative relation of salinity and distance from stream, as well as a positive relation of salinity and elevation change. These two variables were also found to be most important in the partial least squares model used to generate the prediction raster (Fig. 7).

Generally, salinity predictions are within the range of observed values, from 0 to 50 ppt, with a few exceptions. Notably, some predicted salinity values were negative (as the model was not constrained by upper or lower bounds) and set to zero post-modelling. Exceptionally high salinity values (> 70 ppt) were calculated for the April dataset, which may be an artifact resulting from the relatively more poorly constrained April calibration curve (Fig. 5 c) or erroneous field measurements.

In September, the lowest soil salinity is found in the ecotone blocks and at higher elevation areas fringing the marsh. Since the highest elevation areas at Hester marsh are also farthest from tidal channels and experienced the most negative elevation change, it is difficult to

disentangle the importance of each individual factor for soil salinity. Nevertheless, a PLSR model excluding elevation change showed larger error (RMSEP = 6.2) and lower predictive power (R^2= 0.82) than the model including this predictor. Specifically, the variable 'elevation change' contributes to the second PLSR component, covering more of the variance in the predictor space, while reducing the importance of the predictor 'elevation'. This suggests that an underlying process associated with elevation change controls salinity beyond the effect of marsh elevation alone. Surface soils in the west of Hester marsh that are now exposed were covered by several meters of soil before restoration took place. In lieu of detailed data on soil characteristics, it can be assumed that biogeochemical conditions of the now exposed soil change over time. For example, more frequent inundation by seawater does not only directly deliver cation-anion pairs, but can also gradually change soil pH, buffer capacity, and cation exchange capacity, all of which potentially affect apparent conductivity (Kirk, 2004). It was shown that previously dry soils, upon submergence, alter cation concentrations through exchange between solid and liquid phases over time spans of several months, with changes in microbial metabolism on similar time scales (Kirk, 2004). Moreover, a marsh soil transplantation experiment found that the microbial community in freshwater marsh cores did not resemble that of saltmarsh cores even after a year of transplantation into a saltmarsh (Dang *et al.*, 2019). Monitoring of the soil properties mentioned above, as well as the composition of the microbial community, could help identify long-term soil biogeochemical processes that are responsible for the patterns in soil salinity associated with elevation change. Beyond the issue of soil salinity, potential long-term changes in biogeochemical soil properties could also affect the success of plant recruitment. Although this report does not present direct evidence of such processes, it suggests that soil salinity is affected by the depositional history of the sediment used at Hester marsh, inviting similar hypotheses to be tested with regards to plant recruitment.

Future estimations of soil salinity at Hester marsh could potentially follow the model framework established herein, using updated field measurements of apparent conductivity to derive salinity maps. Future conductivity measurements should be accompanied by soil sampling for the generation of new calibration curves, as differences between months were apparent here and would be expected in the future. It is conceivable that, with data from more time points, an overall calibration curve for Hester marsh soil could be generated, which would allow for quick salinity predictions from field measurements without the need for further laboratory analyses.

However, great care should be taken that field measurements are comparable, ensuring consistency in instrument settings (vertical/horizontal, coil spacing) and operation (zero on site, hold at specific height above soil).

The workflow presented in this report is suitable for monitoring soil salinity and produces data with high spatial resolution without extensive field and laboratory work required, by using a portable conductivity meter and UAV. Fitting the UAV with a sensor that records NIR allows for the generation of spectral indices (NDVI, SMI). Soil moisture was shown to correspond with apparent conductivity readings (see Fig. 4), but the SMI calculated here could be improved upon by inclusion of a short-wave infrared band, hence such sensor should be used on the UAV, if available. Since soil property information is generated together with maps of vegetation health (NDVI), it is possible to extend the present analysis to monitor plant recruitment and test for effects of soil properties on plant health. Particularly the calculation of vegetation height at different time points can give insights into development of marsh vegetation over time. In the case of a marsh restoration project that includes the addition of sediments from multiple sources, additional sampling of soil characteristics at several time points could give insight into long-term biogeochemical processes that might be relevant for plant recruitment but cannot be revealed by remote sensing techniques alone.

Conclusion

The present study used a portable conductivity meter (EM38 MK2) to measure bulk apparent conductivity of soils at a tidal marsh restoration site that was recently treated with thin layer deposition of sediment. Soil samples of the top 10 cm were analyzed for salinity in the laboratory, using a 1:5 soil to water ratio, yielding a strong correlation of apparent conductivity and salinity. An aerial survey with multispectral sensors allowed for the generation of an elevation model, vegetation, and soil moisture indices. Together with spatial information of past elevation change and distance to tidal channels, these data products served as predictors of

conductivity in a partial least squares regression model, resulting in a map of predicted conductivity. The workflow presented herein shows promise to reveal spatial and temporal patterns in marsh soil salinity, a potentially important driver of colonization by salt marsh vegetation.

Associated Files

- Conductivity measurements and modelled Salinity (2019 Salinity at Hester Marsh in April and September.xlsx)
- Model Raw Data (All_point_locations.csv)
- Multispectral Orthomosaic (Multispectral.tif)
- Raster Files (Predicted Salinity.tif, DEM.tif, NDVI.tif, SMI.tif, Dist.tif, Scraping.tif)
- Figures 1 – 8 (Fig X.png)

References

Bertness, M. D. (1991) 'Zonation of Spartina Patens and Spartina Alterniflora in New England Salt Marsh', *Ecology*, 72(1), pp. 138–148. Available at: internal-pdf://0740585534/1938909.pdf.

Corwin, D. L. and Lesch, S. M. (2005) 'Apparent soil electrical conductivity measurements in agriculture', *Computers and Electronics in Agriculture*, 46(1-3 SPEC. ISS.), pp. 11–43. doi: 10.1016/j.compag.2004.10.005.

Costanza, R. *et al.* (1997) 'The value of the world's ecosystem services and natural capital', *Nature*, 387(6630), pp. 253–260. Available at: internal-pdf://0446977326/out.pdf.

Craft, C. *et al.* (2009) 'Forecasting the effects of accelerated sea-level rise on tidal marsh ecosystem services', *Frontiers in Ecology and the Environment*, 7(2), pp. 73–78. doi: 10.1890/070219.

Dang, C. *et al.* (2019) 'Novel microbial community composition and carbon biogeochemistry emerge over time following saltwater intrusion in wetlands', *Global Change Biology*, 25(2), pp. 549–561. doi: 10.1111/gcb.14486.

Van Dyke, E. and Wasson, K. (2005) 'Historical ecology of a central california estuary: 150 Years of habitat change', *Estuaries*, 28(2), pp. 173–189. doi: 10.1007/BF02732853.

Fabre, S., Briottet, X. and Lesaignoux, A. (2015) 'Estimation of soil moisture content from the

spectral reflectance of bare soils in the 0.4–2.5 μm domain', *Sensors (Switzerland)*, 15(2), pp. 3262–3281. doi: 10.3390/s150203262.

Hijmans, R. J. *et al.* (2019) 'Package " raster " R topics documented :' Available at: https://cran.r-project.org/package=raster.

James, M. R. and Robson, S. (2014) 'Mitigating systematic error in topographic models derived from UAV and ground-based image networks', *Earth Surface Processes and Landforms*, 39(10), pp. 1413–1420. doi: 10.1002/esp.3609.

Kennish, M. J. (2001) 'Coastal Salt Marsh Systems in the U.S.: A Review of Anthropogenic Impacts', *Journal of Coastal Research*, 17(3), pp. 732–748. Available at: internal-pdf://0107296311/4300224.pdf.

Kirk, G. (2004) *The Biogeochemistry of Submerged Soils*, *The Biogeochemistry of Submerged Soils*. doi: 10.1002/047086303x.

Kuhn, M. (2008) 'Building predictive models in R using the caret package', *Journal of Statistical Software*, 28(5), pp. 1–26. doi: 10.18637/jss.v028.i05.

McKinney, R. *et al.* (2019) 'Seasonal variation in apparent conductivity and soil salinity at two Narragansett Bay, RI salt marshes', *PeerJ*, 2019(11), pp. 1–21. doi: 10.7717/peerj.8074.

McNeill, J. D. (1980) 'Electromagnetic Terrain Conductivity Measurement at Low Induction Numbers', *Technical note TN*, p. 13. Available at: http://www.geonics.com/pdfs/technicalnotes/tn6.pdf.

Pebesma, E. and Bivand, R. S. (2005) 'S Classes and Methods for Spatial Data : the sp Package', *Economic Geography*, 50(1), pp. 1–21. Available at: http://citeseerx.ist.psu.edu/viewdoc/download?doi=10.1.1.160.9361&rep=rep1&type=pdf.

Wehrens, R. and Mevik, B.-H. (2007) 'The pls Package: Principal Component and Partial Least Squares Regression in R', *Journal of Statistical Software*, 18(2).